Chromatic-Dispersion Monitoring Using an Optical Delay-and-Add Filter

Kuen Ting Tsai and Winston I. Way, *Fellow, IEEE*

***Abstract*—A novel postdetection method based on an optical delay-and-add filter (DAF) is proposed for dispersion monitoring at 40 Gb/s or beyond. The proposed method can be used with or without a pilot tone and works well even when there exists a residual chirp due to the finite direct current (DC) extinction ratio of a Mach–Zehnder (MZ) modulator or self-phase modulation (SPM). Several modulation formats, including conventional nonreturn to zero (NRZ), return to zero (RZ), carrier-suppressed RZ (CSRZ), RZ differential phase shift keying (RZ-DPSK), and CSRZ-DPSK are used to numerically demonstrate the feasibility of this technique without using a pilot tone.**

***Index Terms*—Automatic dispersion equalization, fiber chromatic dispersion, optical performance.**

I. Introduction

ONLINE automatic dispersion-equalization techniques are indispensable for long-haul high-speed dense wavelength division multiplexing (DWDM) systems. A dispersion equalizer has two important design parameters, i.e., dispersion monitoring window and dispersion resolution. The dispersion monitoring window is important because a large chromatic-dispersion variation could be incurred due to a wide ambient-temperature change. For example, assuming that the temperature dependence of a zero-dispersion wavelength and the dispersion slope of a 500-km optical fiber system are 0.03 nm/°C and 0.08 ps/nm^2/km, respectively, a temperature change of 40 °C could induce a large dispersion variation of 48 ps/nm. This variation could be even larger for longer transmission distances. Dispersion resolution is of special importance for data rates higher than 40 Gb/s, because a small chromatic dispersion of 60 and 15 ps/nm can cause a 1-dB power penalty in 40 and 80 Gb/s nonreturn-to-zero (NRZ) systems. Modulation formats such as return to zero (RZ) and carrier-suppressed RZ (CSRZ) have even smaller dispersion tolerance, e.g., 40-Gb/s RZ and CSRZ incur a 1-dB power penalty at a chromatic dispersion of 30 [1] and 25 ps/nm [2], respectively.

In a linear dispersion-compensation scheme, residual fiber dispersion could be fully compensated via either a predetection or a postdetection scheme in combination with a variable dispersion compensator (VDC) at a receiver, as illustrated in Fig. 1. In a predetection scheme, a dispersion detector first detects the total chromatic dispersion in a transmission system, and followed by a VDC whose dispersion is adjusted to be the same as the measured total system dispersion but with a negative sign. Examples of predetection schemes include the use of an amplitude-modulation (AM) pilot tone [3], [4] and clock fading technique [1], [5]–[7]. In a postdetection scheme, a zero-dispersion detector is used to monitor the residual dispersion. The zero-dispersion detector generates a VDC control signal so that the VDC can completely cancel the residual dispersion. Examples of postdetection schemes include phase modulation (PM) pilot tones [4], [8], offline alternating chirp [9], and clock-generation techniques [1], [5], [7].

In this paper, we propose a novel postdetection technique that exhibits both sufficient monitoring window and high dispersion resolution. The technique uses an optical delay-and-add filter (DAF), in combination with a) an AM pilot tone or b) any modulation format that has a symmetric spectrum with respect to its optical carrier [e.g., NRZ, RZ, CSRZ, RZ differential phase shift keying (RZ-DPSK), CSRZ-DPSK, etc.]. A DAF is basically an asymmetric Mach–Zehnder interferometer (AMZI) with a differential optical delay τ between the two arms. The DAF used in our proposal has a nominal delay that is equal to a half period of an AM pilot tone or a half-bit/one-bit period of high-speed modulating data when there is no pilot tone.

II. Operation Principle of AM Pilot-Tone-Based Postdetection Scheme Using DAF

A simplified system model is considered in Fig. 2. An optical source [denoted by its electric field $s(t)$, representing a continuous-wave (CW) laser externally modulated by an AM pilot tone with a frequency $f_{\rm p}$] is launched into a dispersive fiber with a transfer function $H_{\rm fiber}(f)$. Only linear dispersion effect is taken into account in this section. The signal at the end of the transmission link is coupled into a DAF, whose constructive or destructive output port has a transfer function $H_{+}(f)$ or $H_{-}(f)$. The received $r_{+}(t)$ or $r_{-}(t)$ after the DAF is converted to a photocurrent $i(t)$. It should be noted that the actual modulating data do not pass through DAF, only the postdetection path passes through the DAF via a tap coupler, as shown in Fig. 1(b). The Fourier transforms of all signals are also shown in Fig. 2. Note that we ignore the effect of baseband modulation in our calculation because we assume any intermodulation product caused by the beating between the baseband data and the pilot tone would have amplitude much smaller than that of the pilot tone. The effect of pilot tone on data can be small [3] and is not within the scope of this paper.

It is well known that after a transmission link and a photoreceiver (without DAF), the magnitude of an AM pilot tone will change with the total accumulated dispersion of the optical link.

Manuscript received September 13, 2004; revised June 28, 2005.

K. T. Tsai is with the Department of Communications Engineering, National Chiao-Tung University, Hsinchu 300, Taiwan, R.O.C.

W. I. Way is with the OpVista Inc., Irvine, CA 92618 USA.

Digital Object Identifier 10.1109/JLT.2005.856230

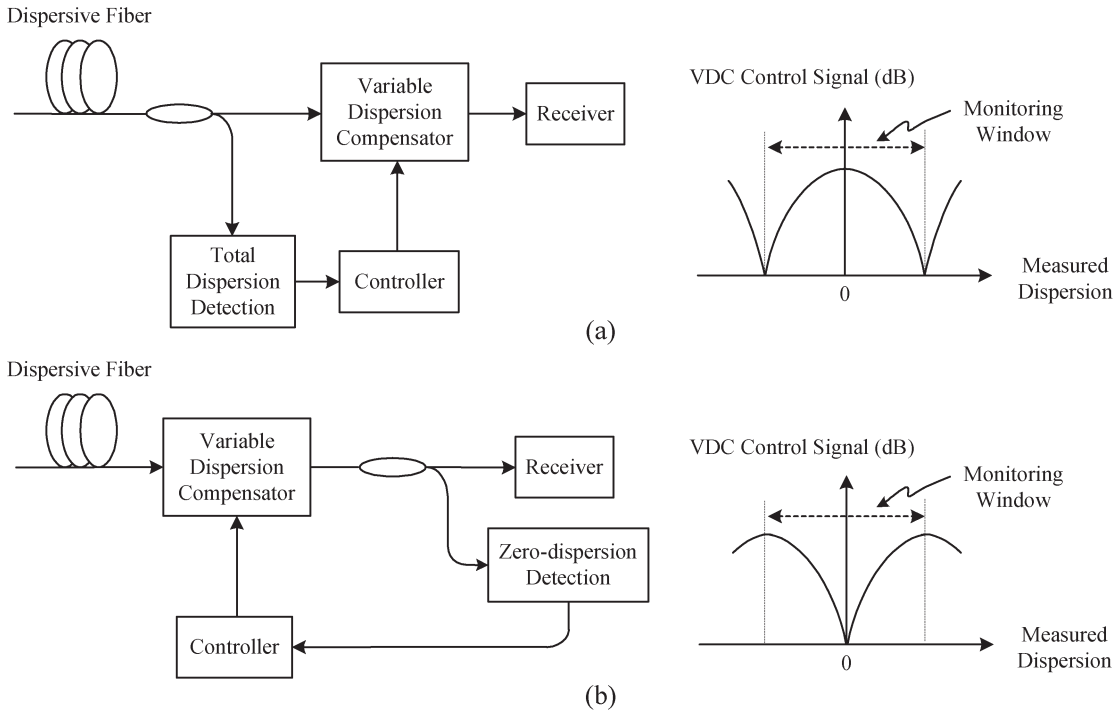

Fig. 1. (a) Predetection and (b) postdetection configurations for a complete dispersion-equalization setup.

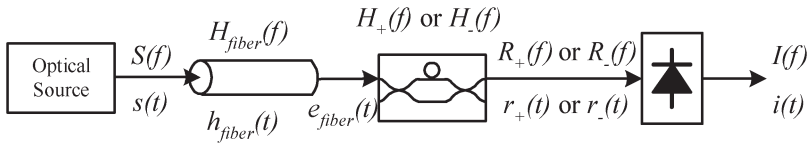

Fig. 2. Simplified block diagram of an optical transmission system with a DAF.

This is because optical fiber dispersion causes a time delay (and thus, relative phase change) between the transmitted upper and lower sideband AM pilot tones. Consequently, in a predetection scheme, we can estimate the total accumulated dispersion by measuring the magnitude of the received pilot tone. The detected chromatic-dispersion-dependent radio frequency (RF) power of an AM pilot tone can be expressed as [10]

$$P_{\mathrm{AM}} = \frac{1}{2}\left\{\Re P_{\mathrm{o}} m \left|\cos\left(\frac{\pi\lambda^2 DL}{c} f_{\mathrm{p}}^2\right)\right|\right\}^2 R_L \qquad (1)$$

where $\Re$ is the responsivity, R_L is the resistive load of the optical receiver, P_{o} is the average received optical power, m is the root mean square (rms) modulation index of the AM pilot tone, c is the speed of light in vacuum, λ is the operating wavelength, D is the fiber dispersion parameter, and DL is the total accumulated dispersion. When the accumulated dispersion is small, the magnitude of the AM pilot tone remains almost constant, and as a result, the frequency of the pilot tone needs to be increased to improve the resolution sensitivity ($\Delta P_{\mathrm{AM}}/\Delta DL$, in decibels per picosecond per nanometer). This out-of-band pilot tone requires a higher bandwidth photodetector and costly microwave/millimeter wave components and reduces the effective system spectral efficiency.

To improve the problems explained above, we use an optical DAF before a photodetector, as shown in Figs. 2 and 3. The frequency response of the constructive port of the DAF can be written as

$$H_+(f) = |H_+(f)|\, \mathrm{e}^{j\Phi_+(f)} = \frac{j}{2}(\mathrm{e}^{-j2\pi\tau f} + 1). \qquad (2)$$

Fig. 4 illustrates the magnitude and phase response of the DAF at the constructive port and the frequency spectrum of an optical carrier (f_{o}) and its associated AM pilot tones ($f_{\mathrm{o}} + f_{\mathrm{p}}$ and $f_{\mathrm{o}} - f_{\mathrm{p}}$). The free spectral range (FSR) of the DAF is $1/\tau$. The basic idea is to let the phase shifts between the optical carrier and the two pilot-tone sidebands be $+\pi/2$ and $-\pi/2$, respectively, so that these two sidebands have a π phase difference, and therefore, they could cancel each other (i.e., the received AM pilot-tone amplitude is 0) when there is zero fiber dispersion. In addition, the received pilot-tone power should change significantly even when only a small residual dispersion is incurred, so that a high dispersion resolution can be obtained. These goals can be achieved when two conditions are satisfied:

1) $\tau = \tau_{\mathrm{o}} = 1/(2f_{\mathrm{p}})$;
2) the left-hand-side pilot tone, the optical carrier, and the right-hand-side pilot tone are aligned with three successive quadrature points of $|H_+(f)|^2$, as shown in Fig. 4, which implies

$$f_{\mathrm{o}} = \frac{2n-1}{4\tau} \qquad (3)$$

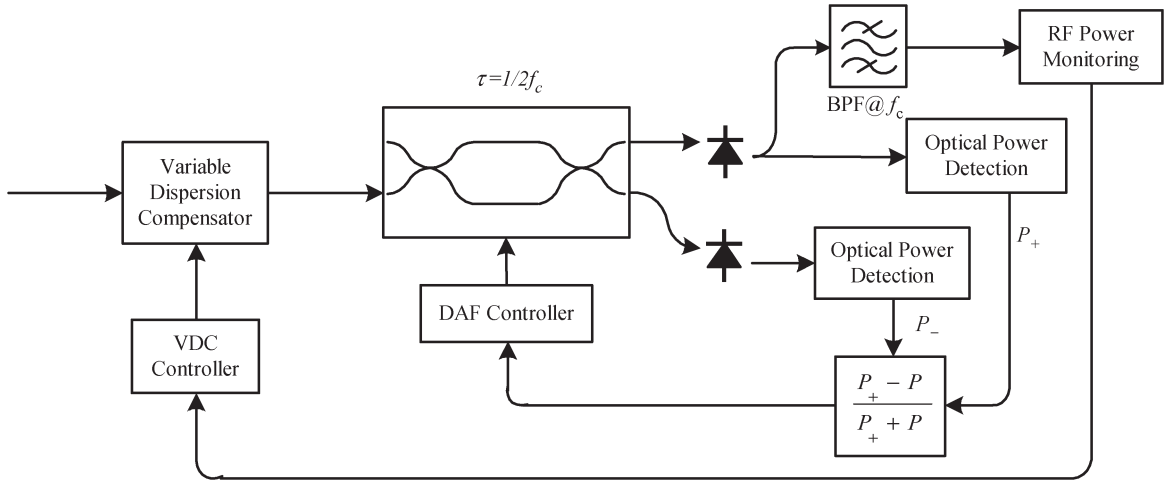

Fig. 3. Complete adaptive dispersion equalizer that is composed of a VDC and the proposed postdetection dispersion monitoring technique. A DAF controller is used to adjust the delay τ to ensure that f_o is aligned with a DAF quadrature point. The VDC is controlled by the monitored clock or pilot-tone RF power, which should be minimized by the VDC.

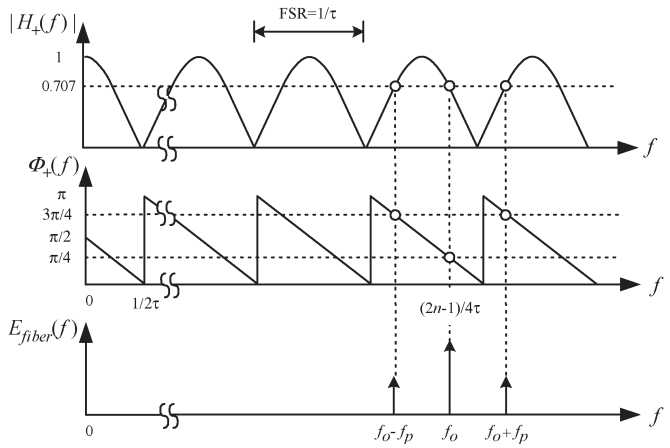

Fig. 4. (a) Optical amplitude and (b) phase responses of a DAF at its constructive port. Also shown is the electric-field spectrum consisting of an optical carrier and its associated pilot tones.

where n is an integer. The amplitudes and phases of the three frequency components in Fig. 4 can be verified by substituting f in (2) with $f_o + 1/(2\tau_o)$, f_o, and $f_o - 1/(2\tau_o)$, respectively, and use the two conditions given above. As a result, the optical carrier and the two pilot tones all experience a 3-dB optical power loss.

It should be noted that in practical systems, τ may deviate away from τ_o, i.e., $\tau = \tau_o + \delta\tau$. This can be observed from the above two conditions that $\tau_o = 1/(2f_p)$ and $\tau = (2n - 1)/(4f_o)$ cannot be always equal for any arbitrary f_o, f_p, and n. As a matter of fact, f_o is always given, while τ needs to be adjusted such that condition 2) is always satisfied, but not necessarily condition 1). For example, if $f_o = 193.3$ THz and $f_p = 40$ GHz, we obtain $\tau = \tau_o = 1/(2f_p) = 12.5$ ps, and (3) is satisfied by letting n equal to 4833. But when the optical carrier frequency is changed to $f_o = 191.123$ THz, (3) is satisfied by letting n equal to 4799 and $\tau \approx 12.501$ ps, i.e., $\tau \neq \tau_o$ in this case. We will show the effect of $\delta\tau$ in Figs. 5 and 6, as well as in (13).

The electric field of a pilot tone after passing through a dispersive fiber and a DAF can be written as

$$\begin{aligned} r_+(t) = \sqrt{P_o} H_1 e^{j\phi_1} e^{j\Omega_0 t} \\ \times \left\{ 1 + \frac{m}{4} \left(\frac{H_2 + H_3}{H_1} \right) e^{j\left(qf_p^2 - \phi_1 + \frac{\phi_2+\phi_3}{2}\right)} \right. \\ \times \cos\left(\omega_p t + \frac{\phi_2 - \phi_3}{2} \right) + j\frac{m}{4} \left(\frac{H_2 - H_3}{H_1} \right) \\ \left. \times e^{j\left(qf_p^2 - \phi_1 + \frac{\phi_2+\phi_3}{2}\right)} \sin\left(\omega_p t + \frac{\phi_2 - \phi_3}{2} \right) \right\} \end{aligned} \tag{4}$$

where

$$q = -2\pi^2 \beta_2 L = \frac{\pi \lambda^2 DL}{c} \tag{5}$$

$$\begin{aligned} H_1 &= |H_+(f_o)| = |\cos(\pi\tau f_o)| \\ H_2 &= |H_+(f_o + f_p)| = |\cos[\pi\tau(f_o + f_p)]| \\ H_3 &= |H_+(f_o - f_p)| = |\cos[\pi\tau(f_o - f_p)]| \end{aligned} \tag{6}$$

and

$$\begin{aligned} \phi_1 &= \Phi_+(f_o) \\ &= -\pi\tau f_o + \frac{\pi}{2} + \angle\cos(\pi\tau f_o) \\ \phi_2 &= \Phi_+(f_o + f_p) \\ &= -\pi\tau f_o + \frac{\pi}{2} + \angle\cos[\pi\tau(f_o + f_p)] - \pi\tau f_p \\ \phi_3 &= \Phi_+(f_o - f_p) \\ &= -\pi\tau f_o + \frac{\pi}{2} + \angle\cos[\pi\tau(f_o - f_p)] + \pi\tau f_p. \end{aligned} \tag{7}$$

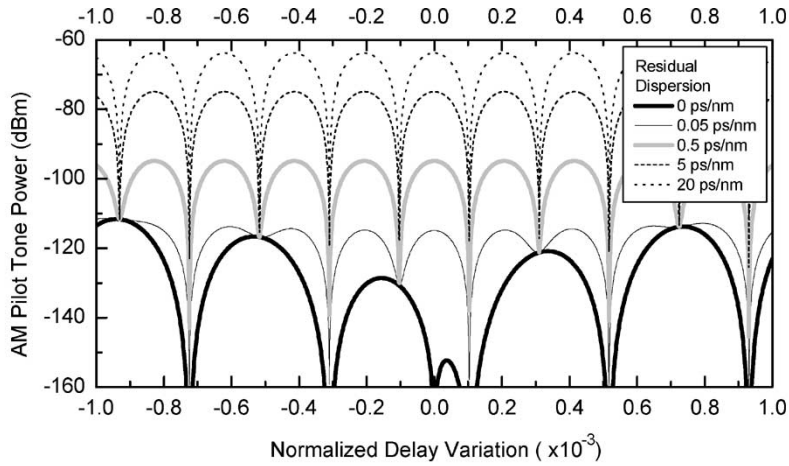

Fig. 5. Power fading effect of an AM pilot tone at 40 GHz due to differential optical delay variation under five accumulated fiber dispersions. The optical wavelength is 193.3 THz ($\sim$ 1552.0 nm), which satisfies (3).

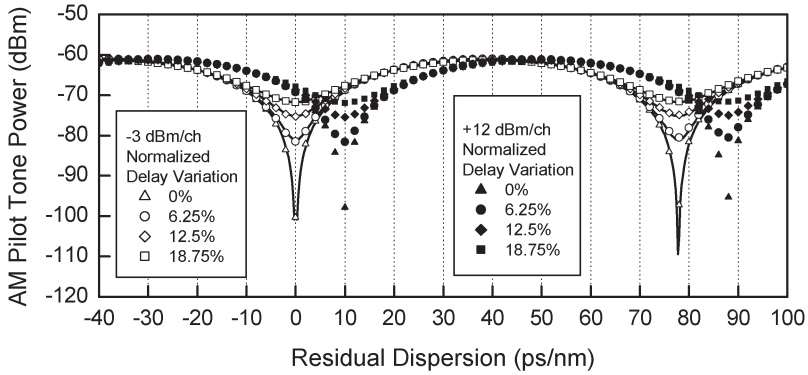

Fig. 6. Calculated (solid lines) and simulated (symbols) AM pilot-tone power as a function of accumulated dispersion with various differential optical delays in solid curves. The optical carrier is at the quadrature point of the power transfer function of the DAF. Simulation parameters are sampling frequency = 1.28 THz, $f_{\rm p} = 40$ GHz, data length = 512 bits, fiber launched power = -3 and 12 dBm/ch, fiber length [single-mode fiber (SMF)] = 50 km, fiber loss = 0.2 dB/km, $D = 16$ ps/nm/km, dispersion slope = 0.08 ps/nm^2/km, fiber nonlinear coefficient = 1.32 W$^{-1}\cdot$km^{-1}, and transmitter MZ modulator extinction ratio = 40 dB. $\delta\tau/\tau_0 = \{0\%, 6.25\%, 12.5\%, 18.75\%\}$, i.e., $\tau = \{1/2/40\text{e}9, 1/2/42.6667\text{e}9, 1/2/45.7143\text{e}9, 1/2/49.2308\text{e}9\}$; and $f_{\rm o} = \{193.28\text{e}12 + 40\text{e}9/2, 193.28\text{e}12 + 42.6667\text{e}9/2, 193.28\text{e}12 + 45.7143\text{e}9/2, 193.28\text{e}12 + 49.2308\text{e}9/2\}$Hz. The choices of $f_{\rm o}$ are to satisfy condition 2) (3) described in Section II.

The photocurrent of $f_{\rm p}$ is obtained by squaring (4) and keeping the linear terms at the modulation frequency $f_{\rm p}$; we arrive at (8) and (9), shown at the bottom of the page. After some mathematical manipulations, it follows that the transfer function of the cascade of a dispersive fiber and a DAF is given by (10), shown at the bottom of the page. Consequently,

$$i_{\rm AM,DAF}(t) = \Re P_{\rm o}\frac{m}{2}H_1\sqrt{(H_2+H_3)^2\cos^2\left(qf_{\rm p}^2-\phi_1+\frac{\phi_2+\phi_3}{2}\right)+(H_2-H_3)^2\sin^2\left(qf_{\rm p}^2-\phi_1+\frac{\phi_2+\phi_3}{2}\right)}$$
$$\times\cos\left(\omega_{\rm p}t+\frac{\phi_2-\phi_3}{2}+\theta\right) \tag{8}$$

$$\text{where } \theta = \tan^{-1}\left\{\frac{(H_2-H_3)\sin\left(qf_{\rm p}^2-\phi_1+\frac{\phi_2+\phi_3}{2}\right)}{(H_2+H_3)\cos\left(qf_{\rm p}^2-\phi_1+\frac{\phi_2+\phi_3}{2}\right)}\right\} \tag{9}$$

$$H_{\rm fib,DAF}(f_{\rm o}+f_{\rm p},\tau,q) = |\cos(\pi\tau f_{\rm o})|\sqrt{\sin^2(\pi\tau f_{\rm o})\sin^2(\pi\tau f_{\rm p})\sin^2(qf_{\rm p}^2)+\cos^2(\pi\tau f_{\rm o})\cos^2(\pi\tau f_{\rm p})\cos^2(qf_{\rm p}^2)} \tag{10}$$

the detected RF power of the AM pilot tone after a dispersive transmission link and a DAF can be expressed as

$$P_{\mathrm{AM,DAF}} = \frac{1}{2}\left\{\Re P_{\mathrm{o}} m H_{\mathrm{fib,DAF}}(f_{\mathrm{o}} + f_{\mathrm{p}}, \tau, q)\right\}^2 R_L. \quad (11)$$

When $\tau = \tau_{\mathrm{o}}$ and (3) are both satisfied, (11) can be simplified as

$$P_{\mathrm{AM,DAF}} = \frac{1}{2}\left\{\Re P_{\mathrm{o}} m K^2 \left|\sin\left(\frac{\pi\lambda^2 DL}{c} f_{\mathrm{p}}^2\right)\right|\right\}^2 R_L \quad (12)$$

where $K = 1/\sqrt{2}$ is the transmittance of the DAF at the wavelength of the pilot-tone sidebands. Comparing (12) to (1), we see that the amplitude of the pilot tone is now related to a sinusoidal function, rather than a cosine function, of the accumulated dispersion. Therefore, the dispersion resolution can be improved significantly around zero dispersion. Note that this sinusoidal dependence on fiber dispersion is similar to those dispersion-equalization techniques that utilize PM pilot tones, i.e., [4] and [8]. The main difference lies in the fact that Youn [4] used a serial PM modulator at the transmitter, Wang *et al.* [8] used a parallel PM modulator at the transmitter, while this paper used an AMZI at the receiver. Therefore, the proposed method in this paper has the same advantages mentioned in [4], such as SPM and polarization mode dispersion (PMD) tolerance. In terms of complexity, the proposed method is not more complicated than those shown in [4] and [8]—those papers have a complicated transmitter design with excessive power loss, while this paper has an extra AMZI at the receiver (note that the tapped loss can be easily compensated by an existing preamplifier). It is also noted that DAFs have been widely used in optical DPSK demodulation and are commercially available with thermally tunable optical delay.

As we mentioned previously, there always will be an unavoidable delay variation $\delta\tau$ in practical conditions. Its effect on an AM pilot-tone RF power at different accumulated fiber dispersion DL can be examined by substituting $\tau f_{\mathrm{o}} = (2n-1)/4$, $\tau = \tau_{\mathrm{o}} + \delta\tau$, and $\tau_{\mathrm{o}} = 1/(2f_{\mathrm{p}})$ into (11) [i.e., condition 2) in Section II is satisfied, while condition 1) is not], which gives us (13), shown at the bottom of the page. Based on (13), Fig. 5 shows the AM pilot-tone power as a function of the normalized delay variation $\delta\tau/\tau_0$ at different total residual dispersion DL (0, 0.05, 0.5, 5, and 20 ps/nm), and $\Re = 1$, $P_{\mathrm{o}} =$ 0.5 mW, $m = 0.16$, $f_{\mathrm{o}} = 193.3$ THz, $f_{\mathrm{p}} = 40$ GHz, and $R_L = 1$. We can see that the maximum AM pilot-tone power always occurs at quadrature points of the DAF power transfer function (i.e., $\delta\tau/\tau_{\mathrm{o}} = 0, \pm 0.021\%, \pm 0.042\%$, etc.) when $DL \neq 0$, and the higher the residual dispersion DL, the higher the AM pilot-tone power. The maximum AM pilot-tone power at $\pm 0.021\%$, $\pm 0.042\%$, etc., can be explained as follows: As previously discussed, $n = 4833$ in (3) when $\tau = \tau_{\mathrm{o}} = 1/(2f_{\mathrm{p}}) = 12.5$ ps. The two nearest quadrature points take place at $n = 4832$ and 4834, respectively. As a result, $\delta\tau/\tau_{\mathrm{o}} = (4834 - 4833)/4833$ or $(4832 - 4833)/4833 = \pm 0.021\%$, if f_{o} is shifted to any of the two neighbor quadrature points. When $DL = 0$, the residual AM pilot-tone power is not completely zero except at several points such as $\delta\tau/\tau_{\mathrm{o}} = 0$. The nonzero residual AM pilot-tone power at $DL = 0$ originates from the $\cos^2(qf_{\mathrm{p}}^2)$ term in the square root of (10) or (13).

Fig. 5 shows a small variation range (within $\pm 0.1\%$) of $\delta\tau/\tau_{\mathrm{o}}$, which means τ_{o} is very closely matching $1/(2f_{\mathrm{p}})$ (this section), or a half of the data-bit period (Section III). However, sometimes due to fabrication uncertainties of τ in AMZI, and sometimes due to data-rate changes after line coding, there may be a large variation range of $\delta\tau/\tau_{\mathrm{o}}$. In Fig. 6, the solid lines are the calculated pilot-tone power as a function of residual dispersion over a much larger variation range of $\delta\tau/\tau_{\mathrm{o}}$ (up to 18.75%) based on (13). In Fig. 6, the frequencies of the pilot tone and optical carrier are 40 GHz and 193.3 THz, respectively; and $\delta\tau/\tau_{\mathrm{o}}$ is set to 0% (open triangle), 6.25% (open circle), 12.5% (open diamond), and 18.75% (open square), respectively. Fig. 6 also shows that the smaller $\delta\tau/\tau_{\mathrm{o}}$, and the smaller the residual dispersion, the higher the dispersion resolution around zero accumulated dispersion. In addition, we see that the monitoring window is ± 39 ps/nm in the 40-GHz pilot-tone-based systems. This monitoring window is sufficient compared to other detection schemes [1], [3]–[7]. Fig. 6 also shows the simulation data (in various symbols) based on VPItransmission Maker. The key simulation parameters are shown in the figure caption of Fig. 6. We can see that these simulation results match well with the theoretically calculated results except that there is a small discrepancy at a normalized delay variation of 0%. This is because the simulation took into account the residual chirp in a transmitter MZ modulator due to its limited extinction ratio of 40 dB, while (13) does not consider the residual chirp. Fig. 6 also shows that a small monitoring error of 10 ps/nm due to SPM is incurred when the fiber launched power is increased from -3 to 12 dBm/ch. As mentioned previously, SPM- and PMD-induced monitoring error can be reduced by lowering the pilot-tone frequency, same as the PM pilot-tone method.

As was shown in Fig. 5, the maximum AM pilot-tone power always occurs at the quadrature points of a DAF power transfer function when $DL \neq 0$. Consequently, the DAF differential delay τ should always be adjusted to let the monitored optical wavelength coincide with one of the DAF quadrature points [i.e., condition 2) (3) in Section II is always satisfied, but not necessarily condition 1)]. We show in Fig. 3 a DAF control loop that can be used to achieve this purpose. This control loop uses a differential optical-power-detection method that is similar to those commonly adapted for wavelength

$$P_{AM,DAF} = \frac{1}{2}\left\{\Re P_{\mathrm{o}} m \frac{1}{2}\sqrt{\cos^2(\pi\delta\tau f_{\mathrm{p}})\sin^2\left(qf_{\mathrm{p}}^2\right) + \sin^2(\pi\delta\tau f_{\mathrm{p}})\cos^2\left(qf_{\mathrm{p}}^2\right)}\right\}^2 R_L \quad (13)$$

stabilization [11]. The DC optical power detected at the constructive and destructive ports are

$$P_+ = P_\mathrm{o}\,|H_+(f_\mathrm{o})|^2 = P_\mathrm{o}\,|\cos(\pi\tau f_\mathrm{o})|^2 = \frac{P_\mathrm{o}}{2}\left\{1+\cos\left[2\pi\tau_\mathrm{o} f_\mathrm{o}\left(1+\frac{\delta\tau}{\tau_\mathrm{o}}\right)\right]\right\} \tag{14}$$

and

$$P_- = P_\mathrm{o}\,|H_-(f_\mathrm{o})|^2 = P_\mathrm{o}\,|\sin(\pi\tau f_\mathrm{o})|^2 = \frac{P_\mathrm{o}}{2}\left\{1-\cos\left[2\pi\tau_\mathrm{o} f_\mathrm{o}\left(1+\frac{\delta\tau}{\tau_\mathrm{o}}\right)\right]\right\} \tag{15}$$

respectively, where $H_+(f)$ was defined in (2), and $H_-(f)$ is the frequency response of the DAF destructive port given by

$$H_-(f) = |H_-(f)|\mathrm{e}^{j\Phi_-(f)} = \frac{1}{2}(\mathrm{e}^{-j2\pi\tau f}-1). \tag{16}$$

The error signal used to stabilize the DAF in Fig. 3 is

$$E = \frac{P_+ - P_-}{P_+ + P_-} = \cos(2\pi\tau f_\mathrm{o}) = \cos\left[2\pi\tau_\mathrm{o} f_\mathrm{o}\left(1+\frac{\delta\tau}{\tau_\mathrm{o}}\right)\right]. \tag{17}$$

It follows that the zero crossings of the error signal occur at

$$\tau = \frac{2n-1}{4f_\mathrm{o}} \tag{18}$$

where n is an integer. This is exactly the same as (3). Note that the control loop uses only the DC optical power of the DAF constructive and destructive ports and is independent of the signal modulation format or data rate.

III. DAF Zero-Dispersion Detection Without a Pilot Tone

In this section, we will show that the DAF postdetection method can also be applied to any modulation format with symmetrical spectrum (e.g., NRZ, RZ, CSRZ, RZ-DPSK, CSRZ-DPSK, etc.). The key point is that when $DL \neq 0$, a clock component $|I(f_\mathrm{c})|$ should be generated, and when $DL = 0$, the clock component should be 0. The DAF used in this section is different from that in Section II in that the differential delay in AMZI is $1/(2f_\mathrm{c})(= T/2$, where T is the data period) instead of $1/(2f_\mathrm{p})$. It should be noted that in Section II, the pilot-tone frequency f_p can be adjusted by a user; while in this section, f_c is the clock frequency of the modulating data, which cannot be changed.

Let us assume that the transmitted electric field $s(t)$ can be expressed as

$$s(t) = x(t)\mathrm{e}^{j\Omega_\mathrm{o} t} \tag{19}$$

where $x(t)$ is the envelope of the electric field and is given by

$$x(t) = \sqrt{\frac{P_\mathrm{o}}{2}}\left[1+\sum_n I_n g(t-nT)\right] \quad \text{[for amplitude shift keying (ASK)]} \tag{20}$$

or

$$x(t) = \sqrt{P_\mathrm{o}}\sum_n I_n g(t-nT) \quad \text{(for PSK)} \tag{21}$$

where $\{I_n\} = \{\pm 1\}$ is the transmitted data sequence, T is the data period, and $g(t)$ is the pulse shape. From (19), we have $S(f) = X(f-f_\mathrm{o})$, where $S(f)$ is the Fourier transform of $s(t)$. $S(f)$ is symmetric with respect to the frequency of the optical carrier, i.e.,

$$\begin{aligned} |S(f_\mathrm{o}+f)| &= |S(f_\mathrm{o}-f)| \\ \phi_s(f_\mathrm{o}+f) &= -\phi_s(f_\mathrm{o}-f) \end{aligned} \tag{22}$$

where $S(f) = |S(f)|\,\mathrm{e}^{j\phi_s(f)}$. We will need to use this symmetric property in deriving (29) later on.

The received optical-signal spectrum before a photodetector is given by

$$R_+(f) = H_+(f)H_\mathrm{fiber}(f)S(f) = |H_+(f)|\,|S(f)|\,\mathrm{e}^{j\{\phi_+(f)+\phi_\mathrm{fiber}(f)+\phi_s(f)\}} \tag{23}$$

where $H_+(f)$ is the transfer functions of a DAF [given by (2), but with τ replaced by $T/2$], and $H_\mathrm{fiber}(f)$ is the transfer function of a dispersive fiber system. The spectrum of the photocurrent is then given by

$$I(f) = R_+(f)\otimes R_+^*(-f) = \int_{f_\mathrm{o}-\frac{1}{2}f_\mathrm{WDM}}^{f_\mathrm{o}+\frac{1}{2}f_\mathrm{WDM}} R_+(\nu)R_+^*(f+\nu)\mathrm{d}\nu \tag{24}$$

where $\otimes$ denotes the convolution operation and f_WDM is the bandwidth of a WDM filter. The clock frequency component at f_c results from the sum of all beats between any two frequency components whose spacing is f_c in the optical spectrum and is given by [with a change of variable $\nu' = \nu + f_\mathrm{c}/2 - f_\mathrm{o}$ in (24)]

$$\begin{aligned} I(f_\mathrm{c}) &= \int_{-\frac{1}{2}f_\mathrm{WDM}+\frac{1}{2}f_\mathrm{c}}^{\frac{1}{2}f_\mathrm{WDM}+\frac{1}{2}f_\mathrm{c}} R_+\left(f_\mathrm{o}+f-\frac{f_\mathrm{c}}{2}\right)R_+^*\left(f_\mathrm{o}+f+\frac{f_\mathrm{c}}{2}\right)\mathrm{d}f \\ &= \int_0^{\frac{1}{2}f_\mathrm{WDM}-\frac{1}{2}f_\mathrm{c}} \left[R_+\left(f_\mathrm{o}-f-\frac{f_\mathrm{c}}{2}\right)R_+^*\left(f_\mathrm{o}-f+\frac{f_\mathrm{c}}{2}\right) + R_+\left(f_\mathrm{o}+f-\frac{f_\mathrm{c}}{2}\right) \times R_+^*\left(f_\mathrm{o}+f+\frac{f_\mathrm{c}}{2}\right)\right]\mathrm{d}f. \end{aligned} \tag{25}$$

Since $R_+(f)$ is composed of $H_+(f)$, $H_\mathrm{fiber}(f)$, and $S(f)$, if we can use their amplitude and phase symmetry/antisymmetry properties (with respect to f_o), and prove that the two terms in (25) are equal and 180° out-of-phase at $DL = 0$, then the usefulness of the DAF detection method is proven. The

amplitude and phase responses, respectively, of the DAF at the constructive port can be expressed as

$$\begin{aligned}&\left|H_+\left(f_\mathrm{o}+f-\frac{f_\mathrm{c}}{2}\right)\right|\\&\quad=\left|H_+\left(f_\mathrm{o}-f-\frac{f_\mathrm{c}}{2}\right)\right|=|\cos(\pi\tau_\mathrm{o}f)|\\&\left|H_+\left(f_\mathrm{o}+f+\frac{f_\mathrm{c}}{2}\right)\right|\\&\quad=\left|H_+\left(f_\mathrm{o}-f+\frac{f_\mathrm{c}}{2}\right)\right|=|\sin(\pi\tau_\mathrm{o}f)|\end{aligned}\tag{26}$$

$$\begin{aligned}&\phi_+\left(f_\mathrm{o}+f+\frac{f_\mathrm{c}}{2}\right)-\phi_+\left(f_\mathrm{o}+f-\frac{f_\mathrm{c}}{2}\right)\\&\quad=\phi_+\left(f_\mathrm{o}-f-\frac{f_\mathrm{c}}{2}\right)-\phi_+\left(f_\mathrm{o}-f+\frac{f_\mathrm{c}}{2}\right)=\theta_+\end{aligned}\tag{27}$$

where $\theta_+ = 90^\circ$ or -90°.

Note that (27) is consistent with the concept presented in Fig. 4, where we have shown that any two frequencies with a difference of f_c (i.e., 0.5FSR) have a phase difference of 90° or -90°. The amplitude response of a dispersive fiber is constant and its transfer function can be expressed as

$$\begin{aligned}H_\mathrm{fiber}\left(f_\mathrm{o}+f+\frac{f_\mathrm{c}}{2}\right)&=H_\mathrm{fiber}\left(f_\mathrm{o}-f-\frac{f_\mathrm{c}}{2}\right)=\mathrm{e}^{jq\left(f+\frac{f_\mathrm{c}}{2}\right)^2}\\H_\mathrm{fiber}\left(f_\mathrm{o}+f-\frac{f_\mathrm{c}}{2}\right)&=H_\mathrm{fiber}\left(f_\mathrm{o}-f+\frac{f_\mathrm{c}}{2}\right)=\mathrm{e}^{jq\left(f-\frac{f_\mathrm{c}}{2}\right)^2}.\end{aligned}\tag{28}$$

Therefore, after substituting (22), (26)–(28) into (25), we can obtain the complex frequency component of the detected signal at f_c as

$$\begin{aligned}I(f_\mathrm{c})=\int_0^{\frac{1}{2}f_\mathrm{WDM}-\frac{1}{2}f_\mathrm{c}}&\Bigg[|\sin(2\pi\tau_\mathrm{o}f)|\left|S\left(f_\mathrm{o}+f+\frac{f_\mathrm{c}}{2}\right)\right|\\&\times\left|S\left(f_\mathrm{o}+f-\frac{f_\mathrm{c}}{2}\right)\right|\\&\times\mathrm{e}^{j\left[\phi_s\left(f_\mathrm{o}+f-\frac{f_\mathrm{c}}{2}\right)-\phi_s\left(f_\mathrm{o}+f+\frac{f_\mathrm{c}}{2}\right)\right]}\\&\times\cos(\theta_++2qf_\mathrm{c}f)\Bigg]\mathrm{d}f.\end{aligned}\tag{29}$$

It follows that at f_c, the magnitude of the complex frequency component $|I(f_\mathrm{c})|$ is 0 if the total accumulated dispersion DL is 0 because the cosine term in (29) is 0 [when $DL = 0$, we have $q = 0$ according to (5), and θ_+ is either 90° or -90°]. Note that this result could be achieved for any real modulating signal that has a symmetric amplitude property (and antisymmetric phase characteristic) with respect to its optical carrier. The simple physics can again be summarized as follows: Since the clock component generated from the beating of any two frequency components with a frequency difference of f_c could result in a phase of $+90^\circ$ or -90°, the resultant clock power after a photodetector is 0 when $DL = 0$, because the number of contributing terms to $+90^\circ$ or -90° is equal. When $DL \neq 0$, however, the upper and lower sideband clock frequencies experience different phase rotations due to the fiber dispersion, the 180° phase relationship no longer exists, and therefore, the resultant clock power after a photodetector is not 0.

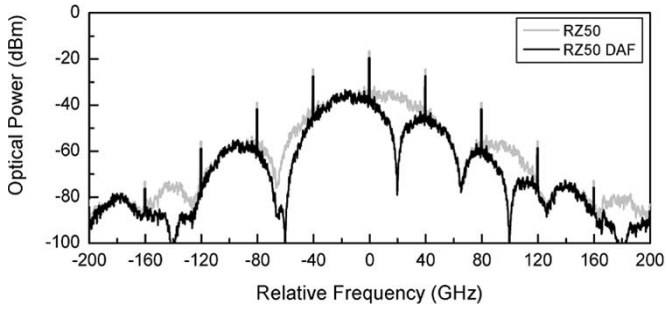

Fig. 7. Simulated optical spectrum of an RZ50 signal without (gray lines) and with (black lines) DAF filtering. The display resolution bandwidth is 625 MHz. Simulation parameters are the same as those in Fig. 6. $\delta\tau/\tau_0 = 0$.

In the case that the modulation formats with asymmetric frequency response are applied, such as an optical single sideband (OSSB) signal, the double-sideband AM pilot-tone-based DAF detection technique (Section II) can be used.

We use an RZ50 signal, which has a symmetrical spectrum with respect to an optical carrier, as an example to show the effectiveness of the DAF approach. The clock extraction is achieved by using a half-bit-delay DAF [$\tau = 1/(2f_\mathrm{c}) = T/2$]. The computer simulation results are shown in Fig. 7 (optical spectrum) and Fig. 8 (RF spectrum). In Fig. 7, the dark and gray lines show the received optical spectrum of an RZ50 signal with and without DAF filtering, respectively, when $DL = 10$ ps/nm. Fig. 8(a) (zero dispersion) and Fig. 8(b) (10-ps/nm dispersion) further illustrate the difference of the detected RF spectra with and without DAF filtering. We can see that when there is no DAF filtering, shown in gray-colored curves, the clock frequency power faded by only about 0.3 dB when the dispersion value is increased to 10 ps/nm. When there is DAF filtering, shown in dark curves, the clock component disappears when there is zero residual dispersion, and its power increases dramatically when the dispersion is increased to 10 ps/nm.

IV. Effects of Modulation Formats, Finite MZI Extinction Ratio, and SPM

In this section, we will show that the proposed technique can work well even when fiber chromatic dispersion interacts with optical frequency chirp, which is caused by a finite DC extinction ratio of an MZ modulator or self-phase modulation (SPM). We will also show the system effects of different pulse shapes [via (29)] using five modulation formats including NRZ, RZ50, CSRZ, RZ-DPSK, and CSRZ-DPSK.

Computer simulations are conducted at a line rate of 40 Gb/s using MZ-modulator-based data and pulse generators, both with an extinction ratio of 40 dB, and the dependence of clock power (after a DAF) on accumulated dispersion is shown in Fig. 9. All transmission parameters are the same as those used in Fig. 6. Two values of $\delta\tau/\tau_0$ (0% and 6.25%) are used. We can see that the clock power for all five modulation formats becomes 0 when there is zero accumulated

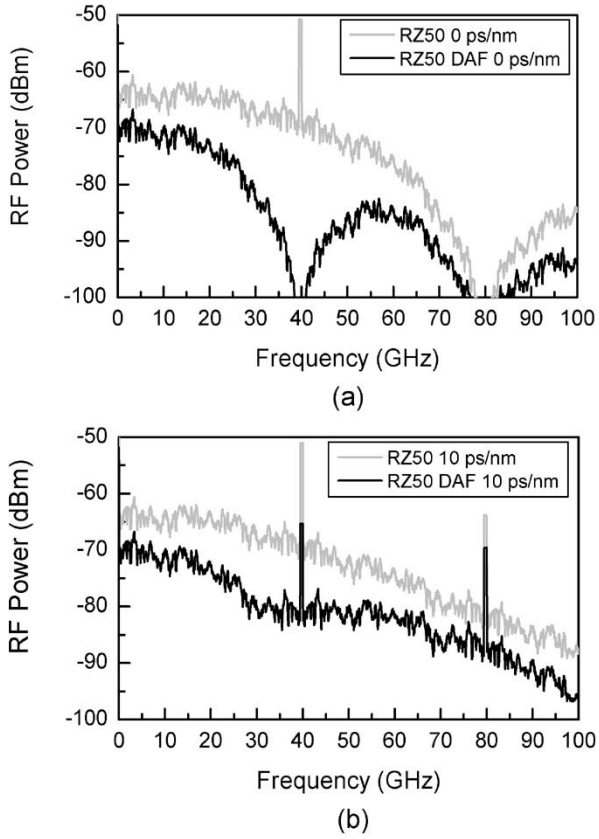

Fig. 8. Simulated RF spectrum of received (a) RZ50 signals under 0-ps/nm dispersion and (b) RZ50 signals under 10-ps/nm dispersion without (gray lines) and with (black lines) DAF filtering, respectively. The display resolution bandwidth is 625 MHz. Simulation parameters are the same as those in Fig. 6. $\delta\tau/\tau_0 = 0$.

dispersion at a zero delay variation. When $\delta\tau/\tau_0 \leq 6.25\%$, the dynamic range of the clock power around zero dispersion is $\geq$ 8 dB for all modulation formats. Here, the dynamic range is defined as the variation range of the detected clock power within the monitoring window. This minimum dynamic range in combination with a dispersion monitoring window of $\sim \pm 30$ ps/nm (slightly smaller than that of the AM pilot-tone-plus-DAF-based method discussed in Section II) for all modulation formats result in a minimum dispersion resolution of $(30\ \text{ps/nm})/(8\ \text{dB}) = 3.75$ ps/nm/dB, which is quite sufficient for the VDC in Fig. 3 to reduce the total dispersion close to 0. Note that CSRZ always has the worst dynamic range around zero dispersion while $\delta\tau/\tau_0 \neq 0$, because the neighbor CSRZ optical pulses have a phase difference of π, which results in an amplitude-cancellation effect.

Four clock-power-detection methods for dispersion equalization are compared in Fig. 10. The four methods are

1) direct detection of the clock power;
2) direct detection of the half-clock power;
3) direct detection of the clock power with a half-bit-delay in DAF;
4) direct detection of the half-clock power with a one-bit-delay in DAF.

We summarize the results of dispersion resolution around zero dispersion and monitoring window in Table I. The "high" dispersion resolution in Table I is defined as $\Delta P/\Delta DL >$

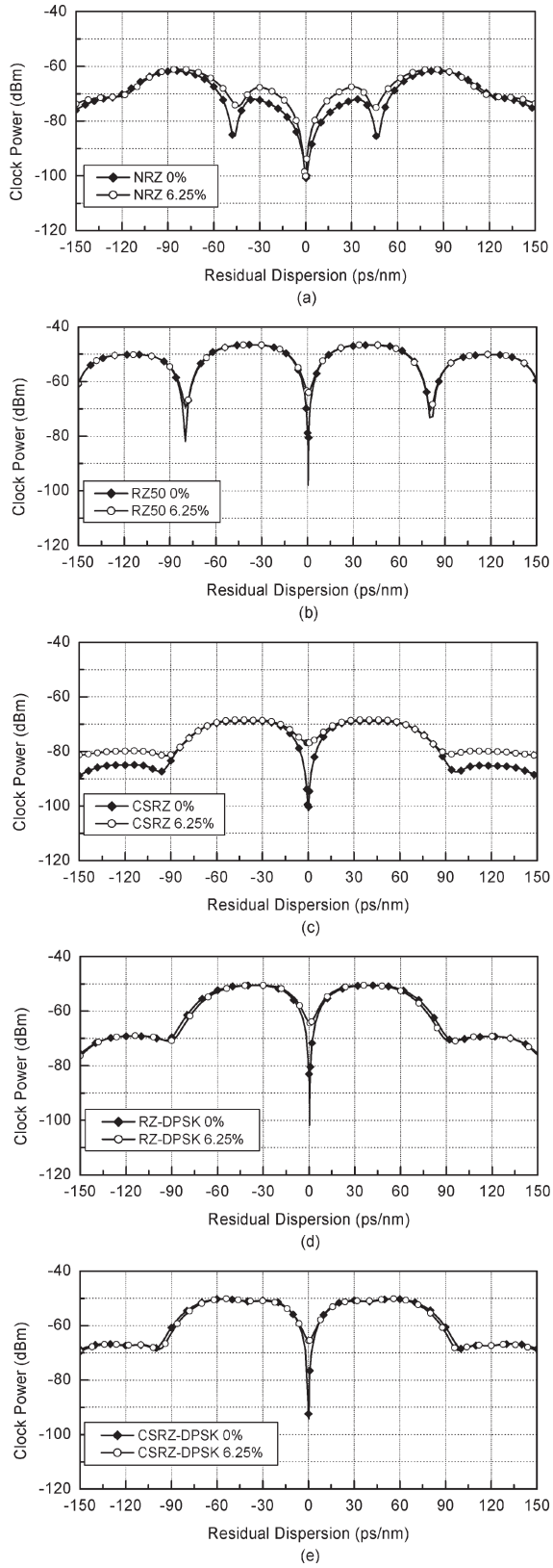

Fig. 9. Clock power after DAF filtering as a function of residual dispersion, with DAF normalized delay variations of 0% and 6.25%, respectively, for 40-Gb/s (a) NRZ, (b) RZ50, (c) CSRZ, (d) RZ-DPSK, and (e) CSRZ-DPSK. All simulation parameters are the same as those in Fig. 6. $f_o = \{193.28\text{e}12 + 40\text{e}9/2, 193.28\text{e}12 + 42.6667\text{e}9/2\}$ Hz for $\delta\tau/\tau_0 = 0\%$ and 6.25%, respectively, which implies that f_o is always aligned with a DAF quadrature point. RF power was detected through a bandpass filter (BPF) at 40 GHz with a 500-MHz bandwidth.

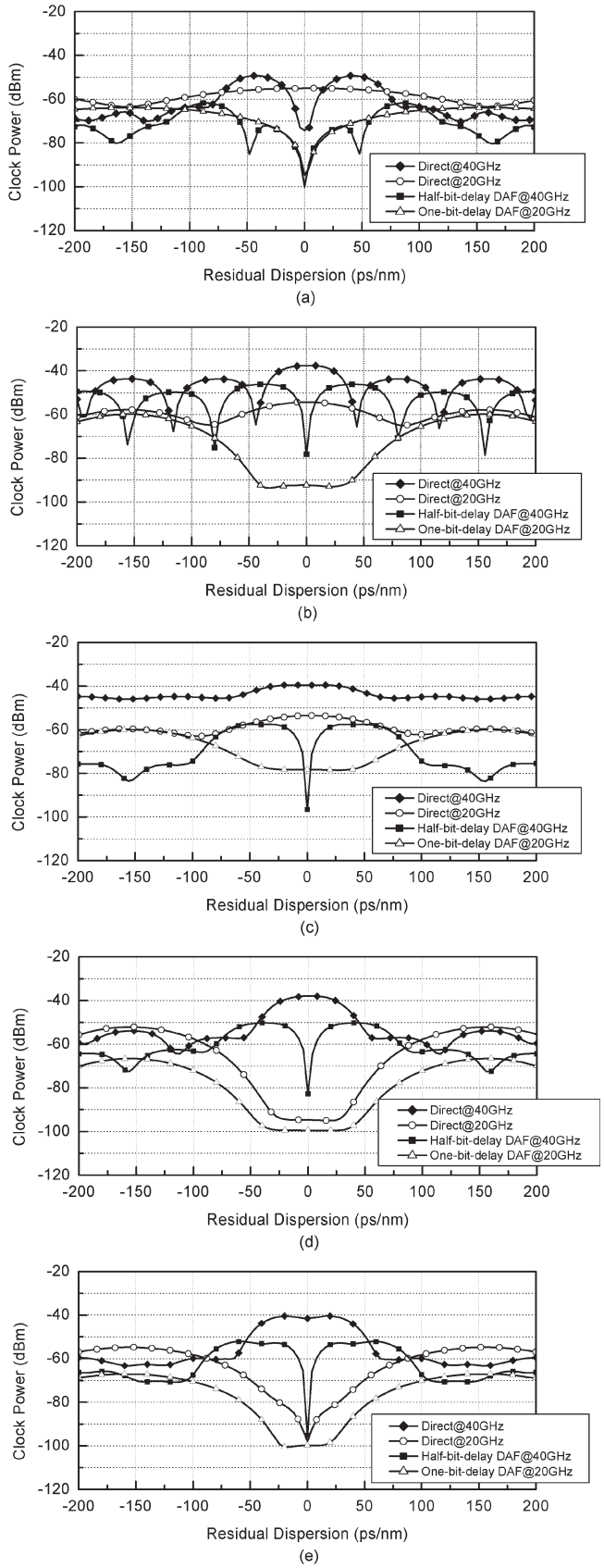

Fig. 10. Clock and half-clock power with and without DAF filtering as a function of residual dispersion, respectively, for 40-Gb/s (a) NRZ, (b) RZ50, (c) CSRZ, (d) RZ-DPSK, and (e) CSRZ-DPSK. All simulation parameters are the same as those in Fig. 6. RF power was detected through a BPF at 20 and 40 GHz, respectively, with a 500-MHz bandwidth.

6 dB within a residual-dispersion window of ± 30 ps/nm. Note that because the residual dispersion is always controlled to be within ± 30 ps/nm, the dispersion penalty for all 40-Gb/s modulation formats under consideration is less than 1 dB. We see that method 3) enables high dispersion resolution for all five modulation formats, while maintaining a relatively high monitoring window (> 56 ps/nm). By lowering the detected clock-power frequency by 50% in method 4), a greater than four times monitoring window of 300 ps/nm (i.e., ± 150 ps/nm) can be achieved. However, most modulation formats can no longer have a good dispersion resolution, except for NRZ. For RZ50 and CSRZ signal formats, one can combine methods 3) and 4) to achieve both a high dispersion resolution and a large monitoring window. For RZ-DPSK, the most cost-effective solution is to combine methods 2) and 3). For CSRZ-DPSK, the direct half-clock-power detection is the best choice, and the DAF method is not needed.

Residual frequency chirp due to a finite modulator DC extinction ratio or SPM is studied next, while a half-bit-delay DAF clock detection technique is used. We use the eye-opening penalty (EOP) to evaluate a system performance, where EOP is defined as [12]

$$\text{EOP(decibel)} = 10\log_{10}\left(\frac{\text{Eye opening back to back}}{\text{Eye opening after transmission}}\right). \tag{30}$$

An EOP of 0.5 and 1 dB represents 90% and 80% eye opening, respectively. In addition, an EOP is estimated using a receiver whose bandwidth is 0.7 times the data rate. All waveforms were simulated without considering optical amplified noise. We assume that a modulator is driven by a 40-Gb/s RZ50 signal with a random word length of 2^9, which corresponds to a frequency resolution of ~ 78 MHz (40e9/512). All simulation parameters are the same as those in Fig. 6. Fig. 11(a) shows the EOP of an RZ50 signal as a function of residual dispersion with various MZ modulators' (both data and pulse generators) DC extinction ratios (20 and 40 dB). We see that the lower the MZ modulator extinction ratio, the more asymmetric is the dispersion penalty curve with respect to zero dispersion. This is because an MZ modulator with a finite DC extinction ratio will always be accompanied by a residual chirp [13], [14], which implies that the phase of an e-field has an initial frequency-chirp term, in addition to the link-distance-dependent chromatic-dispersion phase term (proportional to DLf_c^2). As a result, zero clock power occurs when the initial frequency-chirp-induced phase term is cancelled by a small amount of residual-dispersion-induced phase term, and therefore, zero clock power occurs at a nonzero residual-dispersion value, as shown in Fig. 11(b). We can see that the minimum clock power occurs at the minimum EOP residual dispersion and not at a zero residual dispersion.

Residual frequency chirp could also be generated by SPM [15]. The MZ modulators with extinction ratio of 40 dB are used in the simulation, and the transmission parameters are the same as those used in Fig. 6, except that we purposely increase the fiber launched power to 12 dBm/ch. Fig. 12 shows the EOP (a) and clock power (b) of an RZ50 signal with a

TABLE I
COMPARISON OF DISPERSION RESOLUTION AROUND ZERO DISPERSION AND DISPERSION MONITORING WINDOW OF FIVE MODULATION FORMATS FOR FOUR POWER-DETECTION METHODS AT 40 Gb/s. NOTE THAT "HIGH" DISPERSION RESOLUTION IS DEFINED AS WHEN $\Delta P/\Delta DL > 6$ dB

		NRZ	RZ50	CS-RZ	RZ-DPSK	CSRZ-DPSK
Direct detection @clock	ΔP/ΔDL	High	Low	Low	Low	
	Monitoring Window	± 40 ps/nm	± 40 ps/nm	± 70 ps/nm	± 50 ps/nm	
Direct detection @half clock	ΔP/ΔDL	Low	Low	Low	Low	High
	Monitoring Window	±150 ps/nm	± 75 ps/nm	± 90 ps/nm	±150 ps/nm	±150 ps/nm
Half-bit-delay (12.5 ps) DAF @clock (40GHz)	ΔP/ΔDL	High	High	High	High	High
	Monitoring Window	± 34 ps/nm	± 36 ps/nm	± 34 ps/nm	± 34 ps/nm	± 28 ps/nm
One-bit-delay (25 ps) DAF @half clock (20GHz)	ΔP/ΔDL	High	Low	Low	Low	Low
	Monitoring Window	±150 ps/nm	±150 ps/nm	±150 ps/nm	±150 ps/nm	±150 ps/nm

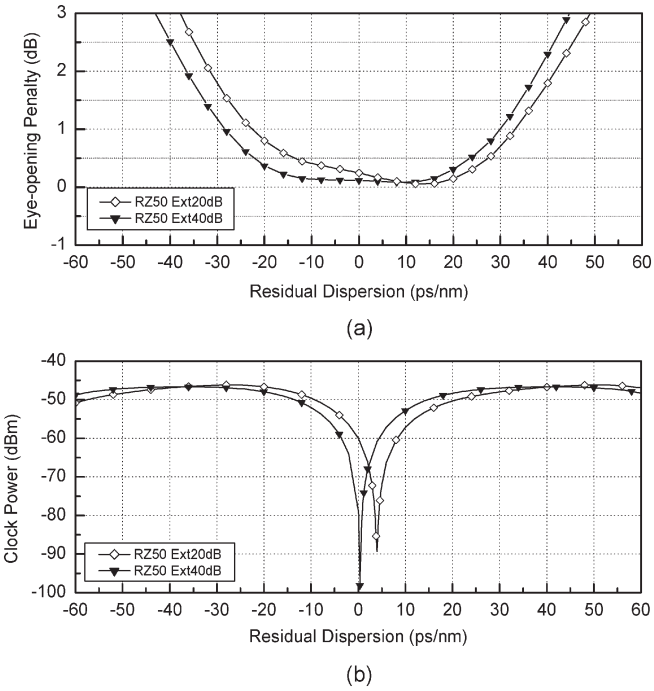

Fig. 11. (a) Simulated EOP and (b) corresponding clock power as a function of residual dispersion with finite MZ modulator DC extinction ratios of 20 dB (open diamond) and 40 dB (down triangle), respectively, for a 40-Gb/s RZ50 signal. Simulation parameters are the same as those in Fig. 6. $\delta\tau/\tau_0 = 0$. RF power was detected through a BPF at 40 GHz with a 500-MHz bandwidth.

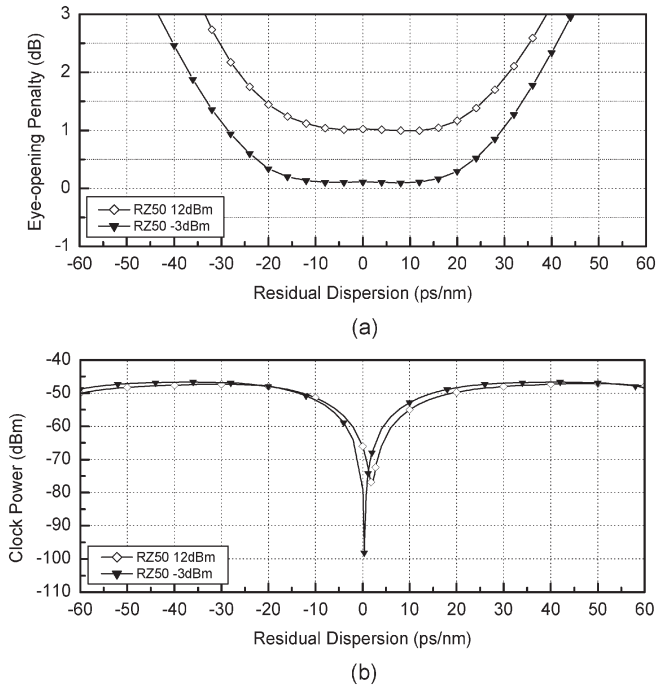

Fig. 12. (a) Simulated EOP and (b) corresponding clock power as a function of residual dispersion with fiber launched power of −3 dBm/ch (triangle) and 12 dBm/ch (open diamond), respectively, for a 40-Gb/s RZ50 signal. Simulation parameters are the same as those in Fig. 6. $\delta\tau/\tau_0 = 0$. RF power was detected through a BPF at 40 GHz with a 500-MHz bandwidth.

launched power of −3 and 12 dBm/ch, respectively. We can see that at a 12-dBm/ch launched power, the minimum EOP and clock power occur at ∼ 2-ps/nm instead of 0-ps/nm residual dispersion. The minimum EOP at 12 dBm/ch is only about 1 dB higher than that at −3 dBm/ch.

V. CONCLUSION

An adaptive postdetection method is proposed for chromatic-dispersion monitoring. The method uses an optical delay-and-add filter (DAF), whose two arms have a differential optical delay equal to a half period of a pilot tone or a

half-data-bit/one-data-bit period. This method does not require a pilot tone if the transmitted data have a symmetrical spectrum with respect to its optical carrier. Adaptive feedback schemes, such as a scheme to accurately align the DAF quadrature point with the optical carrier of a monitored wavelength and a scheme to automatically adjust a variable dispersion compensator (VDC) based on the monitored clock or pilot-tone power, are proposed to form a complete dispersion-equalization apparatus. We have shown that the postdetection scheme works well even when a residual chirp exists due to a finite Mach–Zehnder (MZ) modulator DC extinction ratio or self-phase modulation (SPM). The proposed scheme was also verified by VPI simulation to work well for various modulation formats such as nonreturn-to-zero (NRZ), RZ50, carrier-suppressed RZ (CSRZ), RZ differential phase shift keying (RZ-DPSK), and CSRZ-DPSK. The dependence of the dispersion monitoring window and dispersion resolution on data formats has also been thoroughly studied.

REFERENCES

[1] Z. Pan, Y. Wang, Y. Song, R. Motaghian, S. Havstad, and A. Willner, "Monitoring chromatic dispersion and PMD impairments in optical differential phase-shift-keyed (DPSK) systems," in *Proc. Optical Fiber Communication (OFC)*, Atlanta, GA, Mar. 2003, pp. 402–403, Paper WP1.

[2] S. M. R. M. Nezam, T. Luo, J. E. McGeehan, and A. E. Willner, "Enhancing the monitoring range and sensitivity in CSRZ chromatic dispersion monitors using a dispersion-biased RF clock tone," *IEEE Photon. Technol. Lett.*, vol. 16, no. 5, pp. 1391–1393, May 2004.

[3] M. N. Petersen, Z. Pan, S. Lee, S. A. Havstad, and A. E. Willner, "Dispersion monitoring and compensation using a single inband subcarrier tone," in *Proc. Optical Fiber Communication (OFC)*, Anaheim, CA, Mar. 2001, pp. WH4-1–WH4-3.

[4] C. Youn, "Effects of SPM and PMD on chromatic dispersion monitoring techniques using pilot tones," in *Proc. Optical Fiber Communication (OFC)*, Atlanta, GA, Mar. 2003, pp. 403–404, Paper WP2.

[5] G. Ishikawa and H. Ooi, "Demonstration of automatic dispersion equalization in 40-Gbit/s OTDM transmission," in *Proc. Eur. Conf. Optical Communication (ECOC)*, Madrid, Spain, Sep. 1998, pp. 519–520.

[6] A. Sano, T. Kataoka, M. Tomizawa, K. Hagimoto, K. Sato, K. Wakita, and K. Kato, "Automatic dispersion equalization by monitoring extracted-clock power level in a 40-Gbit/s, 200-km transmission line," in *Proc. Eur. Conf. Optical Communication (ECOC)*, Oslo, Norway, 1996, vol. 2, pp. 207–210.

[7] Z. Pan, Q. Yu, Y. Xie, S. A. Havstad, A. E. Willner, D. S. Starodubov, and J. Feinberg, "Chromatic dispersion monitoring and automated compensation for NRZ and RZ data using clock regeneration and fading without adding signaling," in *Tech. Dig. Optical Fiber Communication (OFC)*, Anaheim, CA, Mar. 2001, pp. WH5-1–WH5-3.

[8] Y. Wang, Z. Pan, A. Sahin, L. Yan, C. Yu, and A. Willner, "In-line chromatic dispersion monitoring using optically-added phase-modulated in-band tones for 10 Gb/s system," in *Proc. Optical Fiber Communication (OFC)*, Atlanta, GA, Mar. 2003, pp. 404–406, Paper WP3.

[9] S. Kuwahara, A. Sano, K. Yonenaga, Y. Miyamoto, and H. Toba, "Automatic dispersion equalization with simple zero dispersion detection using alternating chirp signal in 20-Gbit/s, 400-km transmission experiment," in *Proc. Optoelectronics and Communications Conf. (OECC)*, Beijing, China, Oct. 1999, pp. 383–386.

[10] G. Rossi, T. E. Dimmick, and D. J. Blumenthal, "Optical performance monitoring in reconfigurable WDM optical networks using subcarrier multiplexing," *J. Lightw. Technol.*, vol. 18, no. 12, pp. 1639–1648, Dec. 2000.

[11] K. Tatsuno, M. Shirai, H. Furuichi, K. Kuroguchi, N. Baba, H. Kuwano, Y. Iwafuji, and A. Murata, "50 GHz spacing, multi-wavelength tunable locker integrated in a transmitter module with monolithic-modulator and a DFB-laser," in *Proc. Optical Fiber Communications Conf. (OFC)*, Anaheim, CA, Mar. 2001, pp. TuB5-1–TuB5-4.

[12] A. Hodzic, B. Konrad, and K. Petermann, "Alternative modulation formats in $N \times 40$ Gb/s WDM standard fiber RZ-transmission systems," *J. Lightw. Technol.*, vol. 20, no. 4, pp. 598–607, Apr. 2002.

[13] S. Walklin and J. Conradi, "Effect of Mach-Zehnder modulator DC extinction ratio on residual chirp-induced dispersion in 10-Gb/s binary and AM-PSK duobinary lightwave systems," *IEEE Photon. Technol. Lett.*, vol. 9, no. 10, pp. 1400–1402, Oct. 1997.

[14] H. Kim and A. H. Gnauck, "Chirp characteristics of dual-drive Mach-Zehnder modulator with a finite dc extinction ratio," *IEEE Photon. Technol. Lett.*, vol. 14, no. 3, pp. 298–300, Mar. 2002.

[15] G. P. Agrawal, *Nonlinear Fiber Optics*. San Diego, CA: Academic, 1989.

Kuen Ting Tsai was born in Tainan, Taiwan, in 1975. He received the B.S. and M.S. degrees in communication engineering from the National Chiao-Tung University, Taiwan, in 1997 and 1999, respectively. He is currently working toward the Ph.D. degree in the National Chiao-Tung University with research interests in investigation of modulation formats for DWDM systems and subsystems for optical transmission-system applications.

Winston I. Way (S'82–M'82–SM'88–F'01) received the M.S. and Ph.D. degrees from the University of Pennsylvania, Philadelphia, in 1981 and 1983, respectively.

He was with the Applied Research, Bellcore (now Telcordia), Red Bank, NJ, from 1984 to 1992, where he pioneered research in subcarrier-multiplexed lightwave systems and conducted a number of well-known dense-wavelength-division-multiplexing (DWDM) digital/analog video transmission experiments. From 1992 to 2000, he was a Professor at the National Chiao-Tung University, Hsinchu, Taiwan, R.O.C., where he continued leading many research projects in HFC systems and networks. From 1998 to 2000, he was also a Consultant at Telcordia, conducting reserach on next-generation Internet optical networks. In 2000, he founded OpVista Inc., Irvine, CA, and has been developing ultra-DWDM transmission equipment. He is the author of the book *Broadband Hybrid/Fiber Coax System Technologies* (New York: Academic, 1998), has published more than 100 journal and conference papers, and holds more than a dozen published or pending U.S. patents.

Dr. Way has served on the technical program committees of OFC, MTT, OECC, the IEEE Lasers & Electro-Optics Society (LEOS), and the Optical Society of America (OSA).